RSC Advances

ARTICLE

# Highly Emissive Excited– State Intramolecular Proton Transfer (ESIPT) Inspired 2–(2'–Hydroxy) Benzothiazole –Fluorene Motifs: Spectroscopic and Photophysical Properties Investigation

Received 00th September 2015,
Accepted 00th September 2015

DOI: 10.1039/x0xx00000x

www.rsc.org/advances

**Vikas S. Padalkar, *[a] Daisuke Sakamaki, [a] Norimitsu Tohnai, [b] Tomoyuki Akutagawa, [c] Ken-ichi Sakai [d] and Shu Seki *[a]**

Tuning or switching of the solid state luminescence of organic materials is an attractive target for both basic research and practical applications. In the present study, solid state emissive compounds with very high quantum efficiencies ($\Phi_F$ up to 68%) were achieved by chemical alteration of excited state intramolecular proton transfer (ESIPT) 2–2'–hydroxy benzothiazole (HBT) unit. Five ESIPT inspired compounds based on fluorene were synthesized via Suzuki coupling reaction. Their photophysical properties were studied by means of steady state absorption, emission spectra and time resolved emission method in solid as well as in solution of different polarities. The fluorophores showed absorption in UV region and emission in visible region with large Stokes shift (~ 232 nm). Efficient yellow emissive compounds showed very high quantum yields ($\Phi_F$ = 55–68 %) in solid state, which are the highest quantum yields in solid state to the best of our knowledge, for fluorene based ESIPT molecules. The fluorescence lifetime in solid state is between 3.48–5.21 ns, while it is 5–10 fold less in chloroform (0.52–0.75 ns) solution. The optical properties of these compounds are sensitive towards the polarity of the medium. The structural properties, such as X–ray single crystal analyses, DSC and TGA were studied, and the lack of stacking and/or hydrogen bonding interactions around HBT motifs reveals enough room for ESIPT in the series of molecules even in their solid state. The DFT computations were performed to support experimental results and the calculations are well in line with the experimental results. These suggest high quantum efficiency ascribed to the large orbital energy difference between HOMOs and LUMOs of *enol* and *keto* forms transformed via ESIPT, and hence, singlet energy localization onto the *keto* form. The intra–molecular charge transfer nature between fluorene and HBT units plays a key role for the localization of energy on HBT motifs in their excited states.

## Introduction

Organic solid–state luminescent materials have been attracting considerable interest since past two decades in various fields because of their potential use in high–tech applications[1–7]. Most of the solid–state luminescent materials reported so far are used as organic light emitting diodes[8–11], organic solid state lasers[12,13], organic field–effect transistor[14], nonlinear optics[15,16], organic photovoltaics (OPV)[17], and fluorescent sensors[18,19]. These materials are generally designed from the fluorophores that exhibit excellent fluorescence properties in solution[20,21]. It is well known that in solid state, intermolecular interaction enhances nonradioactive deactivation which quenches the luminescence properties of the materials[22]. This phenomenon is called aggregation–caused quenching (ACQ)[2,23]. Modulating the π–conjugated framework to a twisted packing is an ideal approach to avoid ACQ since molecules with twisted solid – state conformations restrict face–to–face arrangement and avoid strong intermolecular interaction in solid phase[2,23]. Recently a new class of luminescent materials has been reported[20,24-28]. These are non–fluorescent in solution or as an individual molecule but are highly emissive in the solid state after formation of aggregates[20,24–28]. This novel class of compounds is referred to as aggregation–induced emission/ aggregation–induced emission enhancement (AIE/AIEE)[20,24–28]. AIE/AIEE fluorophores are however limited and still remain a challenge for new fluorophore development because unclear mechanism allows aggregation[29]. Organic compounds which are highly emissive in rigid media but non emissive in solution (or weakly emissive) have been raising a lot of interest in optoelectronic devices[20,30]. To obtain highly emissive solid state fluorophores, it is essential

[a] *Department of Molecular Engineering, Graduate School of Engineering, Kyoto University, Nishikyo-ku, Kyoto, 615-8510, Japan*
[b] *Department of Material and Life Science, Graduate School of Engineering, Osaka University,Suita, Osaka 565-0871, Japan*
[c] *Institute of Multidisciplinary Research for Advanced Materials, Tohoku University, Sendai, 980-8577, Japan*
[d] *Department of Bio- & Material Photonics, Chitose Institute of Science and Technology, Chitose 066-8655, Japan.*
*Email: vikaspadalkar@gmail.com (V.S.P), seki@moleng.kyoto-u.ac.jp (S.S).*

Electronic Supplementary Information (ESI) available: NMR spectra, steady state measurements, DSC, TGA and photoelectron yield spectroscopy data of compounds **6a–6e**. DFT calculation using B3LYP/6–31G**(d,p) of compound **6a** (optimized structure of *cis*–enol form: $S_0$ and $S_1$ state), experimental energy levels of HOMO and LUMO of compounds **6a-6d** and X–ray crystallographic data of **6b** CCDC 1410376. See DOI: 10.1039/x0xx00000x

to suppress radiationless deactivation of the excited state of the compounds. Various strategies including RIR, RTICT, RCT, AIE /AIEE and ESIPT process used to obtained solid state emission by controlling non–radiative process[20,22,23,25,31–41].

Excited state intramolecular proton transfer (ESIPT) is a photochemical process that produces a tautomer with a different electronic structure from the original excited form[5,42–44]. It is a four level process in which *enol* form (E) can be changed to *keto* form (K) after photo–excitation by transfer of a proton to the neighboring electronegative atoms through intramolecular hydrogen bonding[42]. On relaxation of excited state *keto* form to the ground state, the *enol* form is recovered by ground state proton transfer (GSIPT)[45]. The pre–requisite for ESIPT is the presence of intramolecular hydrogen bonding between acidic proton (–OH and $–NH_2$) and basic moiety (=N– and –C=O) with suitable geometry[46]. Large Stokes shift (~ 6000–10000 $cm^{-1}$)[42], dual emission[34], ultrafast process[47] and spectral sensitivity to the surrounding medium[48] are the remarkable properties of the ESIPT fluorophores. Dual emission originating from both initial excited form and the proton–transfer tautomer or single emission with large Stokes shift covering the whole visible domain can result in the production of white light[49,50]. White light emitters are used as chemical sensors[43,51–53], lightening materials[54], optoelectronic devices[55] and for fundamental photophysical studies[56–58]. Recently, solid state ESIPT chromophores have been reported by several groups for above maintained applications[21,30,34,59,60]. Till date, commonly used and most studied ESIPT fluorophores are derivatives of 2–(2'–hydroxyphenyl) benzimidazole (HBI)[61–63], 2–(2'–hydroxyphenyl) benzoxazole (HBO)[64–66] and 2–(2'–hydroxyphenyl) benzothiazole (HBT)[46,67–69] due to chemical simplicity and efficient ESIPT properties.

Fluorene and its derivatives are among the most studied electroluminescent materials due to desirable electron transporting properties[70–73]. These materials are used in optoelectronic devices as well as in newer arenas of biotechnology[70–74]. The emission properties of fluorene and its derivatives are tunable by controlling the molecular packing through substitution at 9, 9 or 7, 7' –positions[71]. In present study fluorene has been chosen as luminescent electron donor motif and HBT unit as acceptor. HBT unit helps to achieve the solid state emission by reducing self–absorption due to large Stokes shift between absorption and keto–emission[75]. Two HBT units are introduced at 7,7' –position of fluorene through single bonds. This can help in enhancing emission by restricting the intramolecular rotation around the single bonds between two aromatic rings[21,22]. The purpose of two HBT units is to obtain appropriate molecular packing (*slip–stacking*) instead of face–face–stacking (*H*–packing) for enhancement of solid state emission[22].

## Experimental

### Materials

2,7–Dibromo–9,9–dimethylfluorene, 2,7–dibromo–9,9–dihexylfluorene, 2,7–dibromo–9,9–dioctylfluorene, 9,9–didecylfluorene–2,7–diboronic acid, 5–bromosalicyladehyde, 2–aminothiophenol, 1,2–benzenediamine, 1,3–propanediol, $Pd(PPh_3)_4$, $K_2CO_3$, *n*–BuLi and trimethylborate were purchased from Tokyo Chemical Industries (TCI), Japan. All the solvents used for the synthesis were from Wako Pure Chemical Industries Ltd., Japan. All the reagents were used without further purification.

### Characterizations

All the synthesized compounds were purified by column chromatography on silica gel. Compounds **6a–6d** and **6e** were purified by column chromatography followed by recycle preparative HPLC system (Japan Analytical Industry Co., Ltd., LC–9210NEXT with JaiGel–1H/–2H) using chloroform as eluent. The compounds **6a–6e** were characterized by $^1$H–NMR, $^{13}$C–NMR, MALDI–TOF (Matrix–assisted laser desorption ionization time–of–flight) and elemental analysis techniques. The $^1$H–NMR spectra were recorded on a JEOL 400SS (400 MHz) spectrometer and $^{13}$C–NMR spectra on a JEOL 400SS (100 MHz) spectrometer, and all spectra were recorded in a $CDCl_3$ and DMSO–$d_6$ solvent using TMS as an internal reference standard at room temperature (20 °C). Chemical shifts of NMR spectra are given in parts per million (ppm). Low and high resolution matrix–assisted–laser–desorption/ionization (MALDI) mass spectra (MS) were obtained on Bruker Daltonics FLEX–PC using α–phenylcinnamic acid as a matrix. All steady state absorption spectra were recorded on a JASCO V–570 UV–Vis spectrophotometer. Fluorescence spectra were measured on fluorescence spectrophotometer (F–2700, Hitachi High–Technologies). Relative quantum yield measurements were performed using FP–6500 spectrofluorometer (JASCO). Absolute quantum yields in solid state were measured on FP–6500 spectrofluorometer with an ISF–513 fluorescence integrate sphere unit (JASCO). Photoelectron yield spectroscopy (PYS) experiments were performed on RIKEN Keiki Co., Ltd., model AC–3. The single crystals were obtained by slow evaporation of a mixed solution ($CH_2Cl_2$: Hexane) for **6b** and data collections were performed on a Rigaku R–AXIS–RAPID diffractometer with Cu–Kα radiation (λ = 1.54187 Å) at –150 °C. Thermogravimetric analysis (TGA) was performed with an EXSTAR TG/DTA–7200 system (SII Nano Technology Inc.) using a Pt pan at the ramp rate of 10 °C/min under $N_2$ flow. DSC measurements were performed on a PerkinElmer model DSC 8000 differential scanning calorimeter. Powder-XRD measurements were performed on MiniFlex 600, Rigaku make in the range of $2\theta$ = 2–30°. All theoretical calculations were performed using Gaussian 09 package.

**Synthesis Details**

**9,9–Dimethylfluorene–2,7–bis(trimethylene boronates) 2a**

*n*–BuLi (1.6 M in hexane, 14.49 mL, 22 mmol) was added dropwise into a solution of 2,7–dibromo–9,9–dimethylfluorene **1a** (2 g, 5.71 mmol) in anhydrous THF (40 mL) at –78 °C. The reaction mixture was stirred for 3 h prior to the addition of tri–methyl borate (6.31 mL, 57 mmol) in one portion. The mixture was stirred at –78 °C for 1h after addition of tri–methyl borate and warmed to room temperature and stirred for 20 h. The reaction mass was poured into crushed ice containing 2M HCl (100 mL) with constant stirring. The reaction mixture was extracted with diethyl ether (100 mL × 2) and the combined extracts were evaporated to give yellow colored solid. The obtained solid was refluxed with 1,3–propanediol (1.06 mL, 14 mmol) in 60 mL toluene for 12 h. The reaction mass was concentrated under vacuum and the obtained solid was purified by column chromatography (with silica gel and *n*–hexane–ethyl acetate as the eluent) to obtain a white solid **2a** (Yield after column chromatography: 0.84 g, 41%).

$^{1}$H–NMR (400 MHz, $CDCl_3$): δ ppm 7.83–7.76 (m, 2H), 7.74–7.70 (m, 4H), 4.20–4.17 (t, 8H), 2.10–2.04 (m, 4H), 1.48 (s, 6H).

$^{13}$C–NMR (100 MHz, $CDCl_3$): $\delta$ ppm 153.4, 141.6, 132.6, 127.7, 127.5, 119.6, 62.1, 46.7, 27.5, 27.1.

MALDI–TOF (*m*/*z*): calculated: 362.03, found: 362.36.

**9,9–Dihexylfluorene–2,7–bis(trimethylene boronates) 2b**

*n*–BuLi (1.6 M in hexane, 7.5 mL, 12.0 mmol) was added dropwise into a solution of 2,7–dibromo–9,9–dihexylfluorene **1b** ( 2 g, 4.0 mmol) in anhydrous THF ( 40 mL) at –78 °C. The reaction was stirred for 3 h prior to the addition of methyl borate (4.5 mL, 40 mmol) in one portion. The mixture was stirred at –78 °C for 1h after addition of tri–methyl borate and warmed to room temperature and stirred for 20 h. The reaction mass was poured into crushed ice containing 2M HCl (100 mL) with constant stirring. The reaction mixture was extracted with diethyl ether (100 mL × 2) and the combined extracts were evaporated to give yellow colored solid. The obtained solid was refluxed with 1,3–propanediol (0.76 mL, 10 mmol) in 60 mL toluene for 12 h. The reaction mass was concentrated under vacuum and the obtained solid was purified by column chromatography (with silica gel and *n*–hexane–ethyl acetate as the eluent) to obtain a yellow colored solid **2b** (Yield after column chromatography: 1.4 g, 69%).

$^{1}$H–NMR (400 MHz, $CDCl_3$): $\delta$ ppm 7.73–7.66 (m, 6H), 4.20–4.18 (t, 8H), 2.09–2.06 (m, 4H), 1.99–1.95 (m, 4H), 1.15–0.97 (m, 12H), 0.74–0.70 (m, 6H), 0.70–0.50 (m, 4H).

$^{13}$C–NMR (100 MHz, $CDCl_3$): $\delta$ ppm 150.3, 143.6, 132.5, 127.9, 127.6, 119.2, 62.1, 54.9, 40.6, 40.4, 31.6, 29.8, 27.5, 23.7, 22.7, 14.1.

MALDI–TOF (*m*/*z*): calculated: 502.34, found: 503.12.

**9,9–Dioctylfluorene–2,7–bis(trimethylene boronates) 2c**

*n*–BuLi (1.6 M in hexane, 6.7 mL, 10.8 mmol) was added dropwise into a solution of 2,7–dibromo–9,9–octylfluorene **1c** ( 2 g, 3.6 mmol) in anhydrous THF ( 40 mL) at –78 °C. The reaction was stirred for 3 h prior to the addition of methyl borate (4.0 mL, 36 mmol) in one portion. The mixture was stirred at –78 °C for 1h after addition of tri–methyl borate and warmed to room temperature and stirred for 20 h. The reaction mass was poured into crushed ice containing 2M HCl (100 mL) with constant stirring. The reaction mixture was extracted with diethyl ether (100 mL × 2) and the combined extracts were evaporated to give yellow colored solid. The obtained solid was refluxed with 1,3–propanediol (0.63 mL, 8.71 mmol) in 60 mL toluene for 12 h. The reaction mass was concentrated under vacuum and the obtained liquid was purified by column chromatography (with silica gel and *n*–hexane–ethyl acetate as the eluent) to obtain a yellow liquid **2c** (Yield after column chromatography: 1.8 g, 89%).

$^{1}$H–NMR (400 MHz, $CDCl_3$): $\delta$ ppm 7.74–7.66 (m, 6H), 4.20–4.17 (t, 8H), 2.08–2.06 (m, 4H), 1.98–1.94 (m, 4H), 1.27–0.98 (m, 20 H), 0.84–0.52 (m, 10H).

$^{13}$C–NMR (100 MHz, $CDCl_3$):$\delta$ ppm 150.3, 143.6, 132.3, 127.9, 119.2, 62.1, 54.9, 40.4, 31.8, 30.1, 29.4, 29.3, 22.6, 14.1.

MALDI–TOF (*m*/*z*): calculated: 558.41, found: 558.76.

**9,9–Didecylfluorene–2,7–diboronic acid 2d**

9,9–Didecylfluorene–2,7–diboronic acid was purchased from Tokyo Chemical Industries (TCI), Japan and used for next step without purification.

**9,9–Dimethylfluorene–2,7–bis(5–salicylaldehyde) 4a**

9,9–Dimethylfluorene–2,7–bis–trimethylene boronate **2a** (2.0g, 5.5 mmol), 5–bromosalicyladehyde **3** (3.36 g, 16.7 mmol) and $Pd(PPh_3)_4$ (0.016 g, 0.013 mmol) were added to a mixture of 50 mL degassed toluene (three times) and aqueous (degassed water 10 mL) 2 M $K_2CO_3$ under nitrogen atmosphere. The mixture was stirred at 110 °C for 24 h. After completion of reaction (monitored by TLC) the mixture was cooled to room temperature, and poured into deionized water (200 mL). The aqueous layer was extracted thrice with dichloromethane. The combined organic layers were washed with water and dried over sodium sulfate. The organic layer was concentrated under vacuum, to obtain a white colored solid. The crude product was purified by column chromatography (with silica gel and dichloromethane as the eluent) (Yield after column chromatography: 2.1 g, 88%).

$^{1}$H–NMR (400 MHz, $CDCl_3$): $\delta$ ppm 11.02 (s, 2H), 10.02 (s, 2H), 7.83–7.82 (m, 6H), 7.60–7.53 (m, 4H), 7.11–7.09 (d, 2 H), 1.59 (s, 6H).

$^{13}$C–NMR (100 MHz, $CDCl_3$): $\delta$ ppm 196.8, 161.0, 154.8, 138.7, 138.1, 135.9, 133.7, 131.9, 125.9, 120.9, 120.8, 120.7, 118.2, 47.2, 27.4.

MALDI–TOF (*m*/*z*): calculated: 434.15, found: 434.37.

**9,9–Dihexylfluorene–2,7–bis(5–salicylaldehyde) 4b**

9,9–Dihexylfluorene–2,7–bis–trimethylene boronate **2b** (1.0 g, 1.9 mmol), 5–bromosalicyladehyde **3** (0.79 g, 3.9 mmol) and $Pd(PPh_3)_4$ (0.020 g, 0.017 mmol) were added to a mixture of 50 mL degassed toluene (three times) and aqueous (degassed water 10 mL) 2 M $K_2CO_3$ under nitrogen atmosphere. The mixture was stirred at 110 °C for 24 h. After completion of reaction (monitored by TLC), the mixture was cooled to room temperature, and poured into deionized water (200 mL). The

aqueous layer was extracted thrice with dichloromethane. The combined organic layers were washed with water and dried over sodium sulfate. A white colored solid was obtained after the concentration of organic layers. The crude product was purified by column chromatography (with silica gel and dichloromethane as the eluent) (Yield after column chromatography: 1.0 g, 88%).
$^1$H–NMR (400 MHz, $CDCl_3$): $\delta$ ppm 11.02 (s, 2H), 10.02 (s, 2H), 7.85–7.76 (m, 6H), 7.55– 7.49 (m, 4H), 7.12–7.10 (d, 2 H), 2.06–2.02 (m, 4H), 1.15–1.05 (m, 12H), 0.74–0.72 (m, 10H).
$^{13}$C–NMR (100 MHz, $CDCl_3$): $\delta$ ppm 196.8, 161.0, 151.9, 140.0, 138.4, 135.9, 133.8, 131.9, 125.6, 120.9, 120.8, 120.3, 118.2, 55.4, 40.5, 31.5, 29.7, 23.8, 22.6, 14.2, 14.1.
MALDI–TOF (*m*/*z*): calculated: 574.31, found: 574.65.

**9,9–Dioctylfluorene–2,7–bis(5–salicylaldehyde) 4c**

9,9–Dioctylfluorene–2,7–bis–trimethylene boronate **2c** (3.0g, 5.3 mmol), 5–bromosalicyladehyde **3** (2.77 g, 13.7 mmol) and $Pd(PPh_3)_4$ (0.026 g, 0.022 mmol) were added to a mixture of 50 mL degassed toluene (three times) and aqueous (degassed water 10 mL) 2 M $K_2CO_3$ (10 mL) under nitrogen atmosphere. The mixture was stirred at 110 °C for 24 h. After completion of reaction (monitored by TLC) the mixture was cooled to room temperature, and poured into deionized water (200 mL). The aqueous layer was extracted thrice with dichloromethane. The combined organic layers were washed with water and dried over sodium sulfate. A white colored solid was obtained after the concentration of organic layers. The crude product was purified by column chromatography (with silica gel and ethylacetate and hexane as eluent) (Yield after column chromatography: 3.0 g, 89%).
$^1$H–NMR (400 MHz, $CDCl_3$): $\delta$ ppm 11.03 (s, 2H), 10.03 (s, 2H), 7.84–7.78 (m, 6H), 7.56–7.51 (m, 4H), 7.13–7.11 (d, 2 H), 2.07–2.03 (m, 4H), 1.21–1.07 (m, 20H), 0.80–0.76 (m, 10H).
$^{13}$C–NMR (100 MHz, $CDCl_3$): $\delta$ ppm 196.8, 161.0, 151.9, 140.0, 138.4, 135.9, 133.8, 131.9, 125.6, 120.9, 120.8, 120.3, 118.2, 55.4, 40.4, 31.8, 30.0, 29.2, 23.8, 22.6, 14.1.
MALDI–TOF (*m*/*z*): calculated: 630.37, found: 630.86.

**9,9–Didecylfluorene–2,7–bis(5–salicylaldehyde) 4d**

9,9–Didecylfluorene–2,7–diboronic acid **2d** (3.0 g, 5.0 mmol), 5–bromosalicyladehyde **3** (2.24 g, 11.1 mmol) and $Pd(PPh_3)_4$ (0.015 g, 0.012 mmol) were added to a mixture of 50 mL degassed toluene (three times) and aqueous (degassed water 10 mL) 2 M $K_2CO_3$ (12 mL) under nitrogen atmosphere. The mixture was stirred at 110 °C for 24 h. After completion of reaction (monitored by TLC) the mixture was cooled to room temperature, and poured into deionized water (200 mL). The aqueous layer was extracted thrice with dichloromethane. A white colored solid was obtained after the concentration of organic layers. The crude product was purified by column chromatography (with silica gel and ethylacetate and hexane as eluent 5:95) (Yield after column chromatography: 3.54 g, 94%).
$^1$H–NMR (400 MHz, $CDCl_3$): $\delta$ ppm 11.02 (s, 2H), 10.02 (s, 2H), 7.86–7.76 (m, 6H), 7.55–7.50 (m, 4H), 7.12–7.10 (d, 2 H), 2.06–2.02 (m, 4H), 1.30–1.05 (m, 36H), 0.85–0.81 (m, 10H).
$^{13}$C–NMR (100 MHz, $CDCl_3$): $\delta$ ppm 196.8, 161.0, 151.9, 140.0, 138.3, 135.9, 133.8, 131.9, 125.6, 120.9, 120.8, 120.3, 118.2, 55.4, 40.5, 29.8, 29.7, 29.6, 29.3, 14.1.
MALDI–TOF (*m*/*z*): calculated: 743.07, found: 744.21.

**4,4'–(9,9–Dimethyl–9*H*–fluorene–2,7–diyl)bis(2–(benzo[d]thiazol–2–yl)phenol) 6a**

A mixture of 9,9–dimethylfluorene–2,7–bis(5–salicylaldehyde) **4a** (2.0 g, 4.6 mmol ), aminothiophenol **5** (1.38 g, 11.0 mmol), aq. $H_2O_2$ (3.1 g, 92.0 mmol) and conc. HCl (2.52 g, 69.0 mmol) was stirred in ethanol (50 mL) for 24 h at room temperature (22 °C). After completion of reaction, (monitored by TLC) the brown colored reaction mixture was filtered under vacuum, washed with ethanol and dried. The crude product was purified by column chromatography (ethyl acetate: hexane as eluent). The obtained pure yellow colored solid was further purified by HPLC to obtain **6a** (chloroform as mobile phase) abbreviated as **MF–ESIPT**. (Yield after column chromatography: 1.2 g, 59%).
$^1$H–NMR (400 MHz, $CDCl_3$): $\delta$ ppm 12.60 (s, 2H), 8.03–8.01 (d, 2H),7.95–7.92 (m, 4H), 7.85–7.83 (d, 2H), 7.72–7.69 (dd, 2H), 7.65(d, 2H), 7.61–7.59 (dd, 2H), 7.53–7.51 (m, 2H),7.45–7.43 (m, 2H), 7.22–7.21 (d, 2H) 1.63 (s, 6H).
$^{13}$C–NMR (100 MHz, $CDCl_3$): $\delta$ ppm 169.4, 157.5, 154.7, 151.9, 139.4, 137.9, 133.4, 132.7, 131.9, 126.8, 126.0, 125.7, 122.3, 121.6, 121.1, 120.5, 118.4, 117.0, 47.2, 27.4.
MALDI–TOF (*m*/*z*): calculated: 644.80, found: 645.65.
Elemental Analysis; Mol. Formula: $C_{41}H_{28}N_2O_2S_2$ (Actual: C: 76.37, H: 4.38, S:9.95, N:4.34; Found: C: 76.07, H:4.56, S:9.85, N:4.34)

**4,4'–(9,9–Dihexyl–9*H*–fluorene–2,7–diyl)bis(2–(benzo[d]thiazol–2–yl)phenol) 6b**

A mixture of 9,9–dihexylfluorene–2,7–bis(5–salicylaldehyde) **4b** (0.75 g, 1.3 mmol), aminothiophenol **5** (0.65 g, 5.2 mmol), aq. $H_2O_2$ (0.28 g, 7.8 mmol) and conc. HCl (0.53 g, 1.5 mmol) was stirred in ethanol (20 mL) for 24 h at room temperature (22 °C). After completion of reaction, (monitored by TLC) the yellow colored reaction mixture was filtered under vacuum, washed with ethanol and dried. The crude product was purified by column chromatography (ethyl acetate: hexane as eluent). The obtained pure pale yellow colored solid was further purified by HPLC to obtain **6b** (chloroform as mobile phase) abbreviated as **HF–ESIPT**. (Yield after column chromatography: 0.4 g, 45%).
$^1$H–NMR (400 MHz, $CDCl_3$): $\delta$ ppm 12.60 (s, 2H), 8.03–8.02 (d, 2H),7.95–7.92 (m, 4H), 7.81–7.80 (d, 2H), 7.72–7.69 (dd, 2H), 7.61–7.58 (dd, 2H), 7.55–7.53(m, 4H), 7.45–7.43 (m 2H), 7.23–7.21 (d, 2H), 2.09–2.05 (m, 4H), 1.20–1.05 (m, 12 H), 0.79–0.77 (m, 10H).
$^{13}$C–NMR (100 MHz, $CDCl_3$): $\delta$ ppm 169.4, 157.4, 151.9, 139.9, 139.0, 133.5, 132.7, 131.8, 126.8, 125.7, 122.3, 121.6, 121.1, 120.2, 118.4, 117.0, 55.4, 40.4, 31.5, 29.8, 23.9, 22.7, 14.1.
MALDI–TOF (*m*/*z*): calculated: 785.07, found: 786.00.
Elemental Analysis; Mol. Formula: $C_{51}H_{48}N_2O_2S_2$ (Actual: C: 78.02, H:6.16, S:8.17, N:3.57; Found: C:77.61, H:6.11, S:8.15, N:3.51)

**4,4'–(9,9–Dioctyl–9*H*–fluorene–2,7–diyl)bis(2–(benzo[d]thiazol–2–yl)phenol) 6c**

A mixture of 9,9–dioctylfluorene–2,7–bis(5–salicylaldehyde) **4c** (2.0 g, 3.1 mmol), aminothiophenol **5** (0.95 g, 7.6 mmol), aq. $H_2O_2$ (1.7 g, 50.0 mmol) and conc. HCl (1.15 g, 31.0 mmol) was stirred in ethanol (30 mL) for 24 h at room temperature (22 °C). After completion of reaction, (monitored by TLC) the brown-yellow colored reaction mixture was filtered under vacuum, washed with ethanol and dried. The crude product was purified by column chromatography (ethyl acetate: hexane as eluent). The obtained pure pale yellow colored solid was further purified by HPLC to obtain **6c** (chloroform as mobile phase) abbreviated as **OF–ESIPT**. (Yield after column chromatography: 1.0 g, 37%).
$^1$H–NMR (400 MHz, $CDCl_3$): $\delta$ ppm 12.60 (s, 2H), 8.03–8.02 (d, 2H), 7.95–7.92 (m, 4H), 7.81–7.80 (d, 2H), 7.71–7.69 (dd, 2H), 7.61–7.53 (m, 6H), 7.45–7.41(m, 2H), 7.23–7.21 (d, 2H), 2.08–2.05 (m, 4H), 1.20–1.05 (m, 20 H),che 0.77–0.76 (m, 10H).
$^{13}$C–NMR (100 MHz, $CDCl_3$): $\delta$ ppm 169.4, 157.4, 151.9, 139.9, 139.0, 133.5, 131.8, 126.9, 126.8, 125.7, 122.3, 121.6, 121.1, 120.2, 118.4, 117.0, 55.4, 40.4, 31.8, 30.1, 29.3, 29.2, 22.7, 14.1.
MALDI–TOF (*m*/*z*): calculated: 841.18, found: 842.08.
Elemental Analysis; Mol. Formula: $C_{55}H_{56}N_2O_2S_2$; Elemental Analysis (Actual: C: 78.53, H:6.71, S:7.62, N:3.33; Found: C: 78.46, H:6.74, S:7.62, N:3.39)

**4,4'–(9,9–Didecyl–9*H*–fluorene–2,7–diyl)bis(2–(benzo[d]thiazol–2–yl)phenol) 6d**

A mixture of 9,9–didecylfluorene–2,7–bis(5–salicylaldehyde) **4d** (2.0 g, 2.6 mmol), aminothiophenol **5** (0.75 g, 6.0 mmol), aq. $H_2O_2$ (1.3 g, 32.5 mmol) and conc. HCl (0.91 g, 24.9 mmol) was stirred in ethanol (40 mL) for 24 h at room temperature (22 °C). After completion of reaction, (monitored by TLC) the brown colored reaction mixture was filtered under vacuum, washed with ethanol and dried. The crude product was purified by column chromatography (ethyl acetate: hexane as eluent). The obtained pure pale yellow colored solid was further purified by HPLC to obtain **6d** (chloroform as mobile phase) abbreviated as **DF–ESIPT**. (Yield after column chromatography: 0.8 g, 31%).
$^1$H–NMR (400 MHz, $CDCl_3$): $\delta$ ppm 12.60 (s, 2H), 8.03–8.02 (d, 2H),7.95–7.92 (m, 4H), 7.81–7.79 (d, 2H), 7.69 (dd, 2H), 7.61–7.51 (m, 6H), 7.43–7.40 (m, 2H), 7.21–7.23 (d, 2H), 2.05–2.09 (m, 4H), 1.23–1.09 (m, 36 H), 0.80–0.73 (m, 10H).
$^{13}$C–NMR (100 MHz, $CDCl_3$): $\delta$ ppm 169.4, 157.4, 151.9, 139.9, 139.0, 133.4, 131.8, 126.9, 126.8, 125.7, 122.3, 121.6, 121.1, 120.2, 118.4, 117.0, 55.4, 40.4, 31.9, 31.0, 30.1, 29.7, 29.4, 29.3, 23.9, 22.7, 14.1.
MALDI–TOF (*m*/*z*): calculated: 953.39, found: 954.22.
Elemental Analysis; Mol. Formula: $C_{63}H_{72}N_2O_2S_2$; (Actual: C: 79.39, H: 7.61, S: 6.73, N: 2.94; Found: C: 79.08, H: 7.59, S: 6.53, N: 2.99)

**4,4'–(9,9–Dioctyl–9*H*–fluorene–2,7–diyl)bis(2–(benzo[d]imidazol–2–yl)phenol) 6e**

A mixture of 9,9–dioctylfluorene–2,7–bis(5–salicylaldehyde) **4c** (0.1 g, 0.15 mmol ), 1,2–benzenediamine **5b** (0.048 g, 0.44 mmol), aq. $H_2O_2$ (0.053 g, 1.55 mmol) and conc. HCl (0.030 g, 0.82 mmol) were stirred in ethanol (10 mL) for 24 h at room temperature (22 °C). After completion of reaction, (monitored by TLC) the brown colored reaction mixture was filtered under vacuum, washed with ethanol and dried. The crude product was purified by column chromatography (ethyl acetate: hexane as eluent). The obtained pure pale yellow colored solid was further purified by HPLC to afford **6e** (chloroform as mobile phase). (Yield after column chromatography: 0.050 g, 39%).
$^1$H–NMR (400 MHz, $DMSO_{d6}$): $\delta$ ppm 13.37 (s, 2H), 13.29 (s, 2H), 8.52 (s, 2H), 7.98–7.96(d, 2H), 7.84–7.68 (m, 10H), 7.34–7.29 (m, 4H),7.18–7.16 (d, 2H), 2.08–2.05 (m, 4H), 1.27–1.02 (m, 20 H), 0.68–0.64 (m, 10H).
$^{13}$C–NMR (100 MHz, $CDCl_3$): $\delta$ ppm 158.0, 152.2, 151.8, 139.8, 138.6, 133.6, 131.9, 130.6, 124.6, 123.0, 120.8, 118.2, 113.4, 112.1, 55.5, 31.6, 29.6, 28.9, 23.8, 21.5, 21.4, 14.3.
MALDI–TOF (*m*/*z*): calculated: 806.46, found: 807.94.

## Result and Discussion

**Design and Synthesis of Compounds**

**Scheme 1** illustrates the chemical structures and synthetic route of HBT **6a–6d** and HBI **6e** derivatives. Five ESIPT fluorophores were designed according to the following procedure. HBT and HBI units were introduced into 7,7'–positions of fluorene unit via Suzuki coupling and cyclisation reactions. 9,9–Dialkylfluorene–2,7–bis(trimethylene boronates) **2a–2c** were synthesized from 2,7–dibromo–9,9–dialkylfluorene by *n*–BuLi reaction at –78 °C followed by substitution reaction of trimethylborate and 1,3–propanediol. Boronate esters **2a–2c** and boronic acid **2d** were coupled with 5–bromosalicyladehyde **3** via Suzuki coupling using $Pd(PPh_3)_4$ catalyst under basic medium to obtain 9,9–dialkylfluorene–2,7–bis(5–salicylaldehyde) **4a–4d.** The condensation followed by cyclisation of 9,9–dialkylfluorene–2,7–bis(5–salicylaldehyde) **4a-4d** with *o*–aminothiophenol **5a** or 1,2–benzenediamine **5b** in acidic catalyzed reaction obtained **6a–6d** and **6e** with good yields. All compounds were found to have good solubility in organic solvents; as a result they could be well purified by chromatography techniques for spectral and optical studies (NMR spectra of all compounds are included in the supporting information).

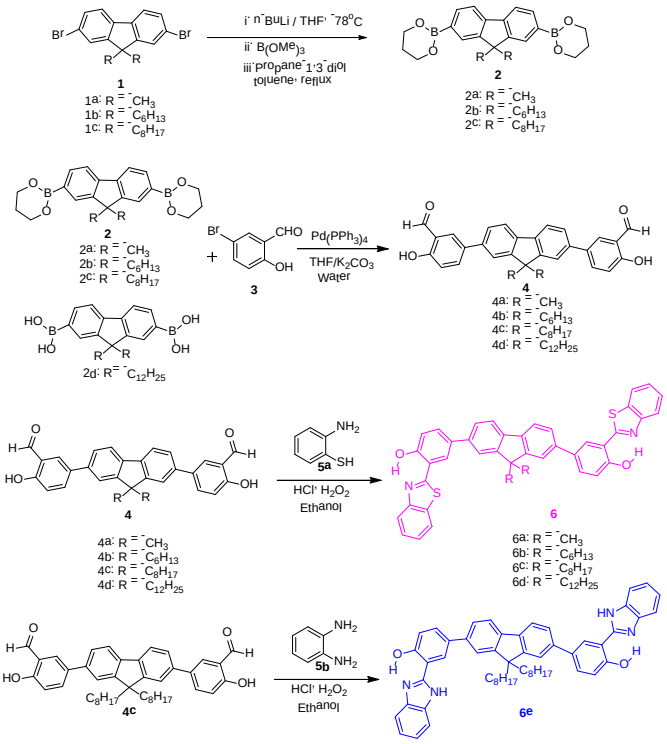

**Scheme 1**: Synthesis of 4,4'–(9,9–dialkyl–9*H*–fluorene–2,7–diyl)bis(2–(benzo[d]thiazol–2–yl)phenol) **6a–6d** and 4,4'–(9,9–dioctyl–9*H*–fluorene–2,7–diyl)bis(2–(benzo[d]imidazole–2–yl)phenol) **6e**.

## Optical Properties

### Steady State measurements

A summary of the steady state absorption and emission of the compounds **6a–6e** is provided in **Table 1.** Compounds **6a–6d** have the same core and differ only by the length of the alkyl chain attached to 9,9–position of the fluorene unit. Initially absorption and emission properties were studied for **HBT**, **6c** and **6e** (**Scheme S1**) to understand the effect of conjugation as well as strength of electron acceptor group on optical properties. **HBT**, **6c** and **6e** showed similar absorption pattern ($\lambda_{abs}$ around 335 nm in chloroform (π–π* transition) (**Fig. 1, Table 1).** However, the emission pattern is totally different. Compound **6c** showed emission at 552 nm which is 62 and 27 nm red shifted emission as compared to benzimidazole **6e** ($\lambda_{em}$ = 490 nm, **Fig. 1**) and HBT ($\lambda_{em}$ = 525 nm) respectively in chloroform. The red shift is explained in terms of more delocalization of the π–electron in **HBT** derivative **6c**, which has more aromatic character in comparison to **HBI** derivative[76]. In ESIPT process, fluorescence properties depend on intra–molecular hydrogen bonding, which occurs at the excited state. In hydroxy–azoles family, the intra–molecular hydrogen bond (OH---N) in HBI was reported to be weak in comparison to HBT[77]. More aromatic character and strong intra–molecular hydrogen bonding enhances the fluorescence properties of the ESIPT fluorophores[21,22,29]. The emission wavelength of **HBT** is almost identical to its derivatives **6a–6d** in chloroform. However it is reported that **HBT** is weakly or non–emissive in crystalline state due to face–face stacking[78]. In present study, synthesized compounds **6a–6d** are highly emissive in crystalline state. This can be assigned for RIR effect and molecular packing of fluorene and HBT unit. Considering the solid state emission with high quantum efficiencies, only HBT based ESIPT fluorophores **6a-6d** were explored for deeper study. The steady state absorption spectra of compounds **6a–6d** in various solvents and on solid film at room temperature are shown in **Fig. 2** and **Fig. S**1.

The absorption spectra of all these compounds in various solvents and on solid film were at 325–344 nm, which can be assigned to the π–π* transition of the fluorene–benzothiazole conjugated backbone of these molecules. In non–polar (toluene and chloroform), polar–protic (methanol) and polar–aprotic (DMF and acetonitrile) solvents, the spectral position of absorption spectra were almost same for all compounds (**Fig. 2** and **Fig. S1**) implying the little influence of solvent polarity on the ground state of these compounds. The similar absorption band of these compounds indicate that these compounds are maintained their *enol* forms at the ground state[67]. In chloroform and toluene absorption maxima was ~ 334 nm, while slightly blue shifted absorption was observed in acetonitrile and methanol solvents. The compounds **6b**, **6c** and **6d** showed 5 nm red shifted absorption in DMF ($\lambda_{abs}$ = 338 nm) as compared to other studied solvents. In the solid state, **6a** showed absorption at 344 nm, which is slightly red shifted (~ 5 nm) compared to **6b**, **6c** and **6d** (**Fig. 2**).

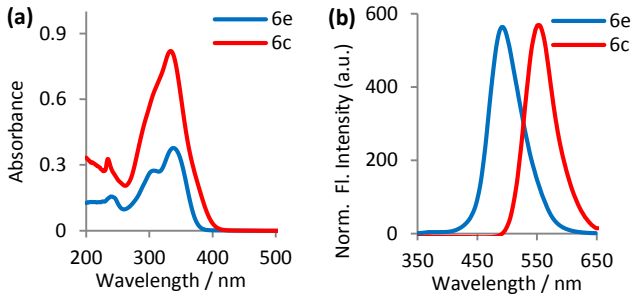


**Fig. 1 (**a) Steady state absorption spectra; (b) fluorescence spectra of compounds **6c** and **6e** in chloroform at room temperature ($10^{-5}$ M concentration; λex = 330 nm for fluorescence measurement).

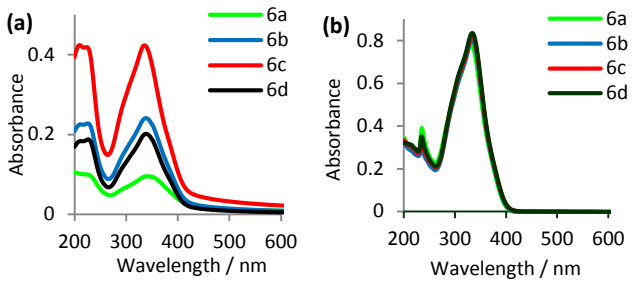


**Fig. 2** Steady state absorption spectra of compounds **6a-6d** (a) in solid state (1 wt %) (b) in chloroform ($10^{-5}$ M concentration) at room temperature.

**Table 1:** Summery of optical properties of the compounds **6a**-**6e** and **HBT**.

| Comps | Medium | $\lambda_{max}^{Abs}$ (nm) | ε (mol$^{-1}$ dm$^3$ cm$^{-1}$) | $\lambda_{max}^{Em}$ (nm) | Stoke shift (nm) | Stoke shift (cm$^{-1}$) | Quantum efficiency $\Phi$ (%) | Fluorescence lifetime (ns) |
|---|---|---|---|---|---|---|---|---|
| 6a | [a] Solid Film | 344 | *g* | 544 | 200 | 10687 | [c] 60.12 | 5.21 |
| | [b] Chloroform | 332 | 78000 | 552 | 220 | 12004 | [d] 1.80, [e] 4.60 | 0.52 |
| | [b] Toluene | 333 | 91500 | 551 | 218 | 11881 | [d] 1.00, [e] 2.90 | *f* |
| | [b] DMF | 336 | 28500 | 415 | 79 | 5665 | [d] 7.90, [e] 7.50 | *f* |
| | [b] Methanol | 329 | 400 | 426<br>527<br>555 | 97<br>198<br>226 | 6920<br>11419<br>12377 | *f* | *f* |
| | [b] Acetonitrile | 331 | 3880 | 407<br>430<br>552 | 76<br>99<br>221 | 5641<br>6955<br>12095 | *f* | *f* |
| 6b | [a] Solid Film | 338 | *g* | 551 | 213 | 11436 | [c] 67.21 | 3.56 |
| | [b] Chloroform | 334 | 80400 | 552 | 218 | 11824 | [d] 1.80, [e] 4.40 | 0.74 |
| | [b] Toluene | 335 | 69400 | 551 | 216 | 11701 | [d] 1.50, [e] 3.10 | *f* |
| | [b] DMF | 338 | 21900 | 415 | 77 | 5489 | [d] 7.50, [e] 7.30 | *f* |
| | [b] Methanol | 325 | 2100 | 412<br>431<br>557 | 87<br>106<br>232 | 6497<br>7567<br>12815 | *f* | *f* |
| | [b] Acetonitrile | 333 | 2300 | 407<br>430<br>543 | 74<br>97<br>210 | 5460<br>6774<br>11613 | *f* | *f* |
| 6c | [a] Solid Film | 336 | *g* | 552 | 216 | 11645 | [c] 54.65 | 3.48 |
| | [b] Chloroform | 334 | 81900 | 552 | 218 | 11824 | [d] 1.70, [e] 4.30 | 0.75 |
| | [b] Toluene | 336 | 72200 | 551 | 215 | 11613 | [d] 1.40, [e] 2.90 | *f* |
| | [b] DMF | 338 | 47200 | 405 | 67 | 4894 | [d] 7.20, [e] 11.50 | *f* |
| | [b] Methanol | 333 | 1560 | 431<br>543 | 98<br>210 | 6828<br>11613 | *f* | *f* |
| | [b] Acetonitrile | 331 | 6230 | 407<br>430<br>552 | 76<br>99<br>221 | 5641<br>6955<br>12095 | *f* | *f* |
| 6d | [a] Solid Film | 339 | *g* | 552 | 213 | 11382 | [c] 62.94 | 3.51 |
| | [b] Chloroform | 334 | 83500 | 552 | 218 | 11824 | [d] 1.60, [e] 4.10 | 0.55 |
| | [b] Toluene | 335 | 70600 | 551 | 216 | 11701 | [d] 1.40, [e] 3.10 | *f* |
| | [b] DMF | 339 | 33300 | 406 | 67 | 4894 | [d] 7.00,[e] 7.40 | *f* |
| | [b] Methanol | 329 | 3700 | 431<br>540 | 102<br>211 | 7193<br>11876 | *f* | *f* |
| | [b] Acetonitrile | 328 | 1940 | 407<br>429<br>552 | 79<br>101<br>224 | 5917<br>7177<br>12371 | *f* | *f* |
| 6e | [b] Chloroform | 335 | 37300 | 490 | 155 | 9442 | *f* | *f* |
| HBT [h] | [b] Chloroform | 338 | *f* | 525 | 187 | 10538 | *f* | *f* |
| | [b] Toluene | 337 | 20100 | 514 | 177 | 10218 | 0.5 | f |
| | [b] Methanol | 332 | 20800 | 373 | 41 | 3310 | f | f |

[a] Measured on thin film, spin-cast from (1 wt %) dichloromethane solution. [b] Measured from $10^{-5}$ M solution. [c] Absolute quantum yields in solid state. [d, e] Quantum yields measured by relative methods using quinine sulphate standard ([d]$10^{-5}$ M and [e]$10^{-6}$ M concentration). [f] Not measured. [g] Not calculated, [h] Literature data[68,88]

Interestingly, the fluorescence properties are solvent dependent. In non–polar organic solvents (toluene and chloroform), compounds showed single broad emission around 552 nm, which is similar to solid state emission (**Fig. 3** and **Fig. S2**). The single broad emission with large Stokes shift can be assigned to the excited state *cis–keto* form (III) (ESIPT emission)[79]. In chloroform and toluene, the strong intramolecular hydrogen bonding stabilizes the ground state ($S_0$) *cis–enol* form (I) and makes up the major population at $S_0$ state. After photoexcitation, *cis–enol* undergoes ESIPT at $S_1$ state to form (II) the excited state *cis–keto* tautomer which then emits at longer wavelength (ESIPT emission) (**Scheme S2**). In polar aprotic and protic solvents (acetonitrile, methanol and DMF) all compounds show significant dual or triple emission (**Fig. S2**). The short wavelength and long wavelength can be assigned to the excited *cis–enol* form (II) and *cis–keto* tautomer (III) respectively. In addition to *cis–enol* and *cis–keto* emission extra emission peak was observed in polar protic and aprotic solvents. The third emission band in methanol could be ascribed to the phenoxide species generated due to deprotonation induced by intermolecular hydrogen bonding between the acidic phenol hydrogen and the solvent molecules form (C)[48] (**Scheme S2**). In acetonitrile, additional peak can be assigned for protonated *cis–enol* form (B)[67]. In polar aprotic solvent (DMF), compounds showed intense emission between 405–415 nm and shoulder peak between 470–480 nm (**Fig. S2**). The *cis–enol* emission was between 405–415 nm and *cis–keto* emission was between 470–480 nm. The short wavelength emission band at 407 nm and long wavelength emission band between 543–552 nm was observed in acetonitrile.

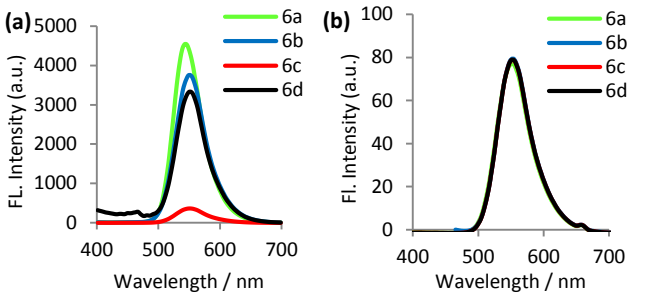


**Fig. 3** Steady state emission spectra of **6a-6d** (a) in solid state (spin coated: 1 wt %) (b) in chloroform ($10^{-5}$ M concentration) at room temperature, λex = 330 nm for fluorescence measurement.

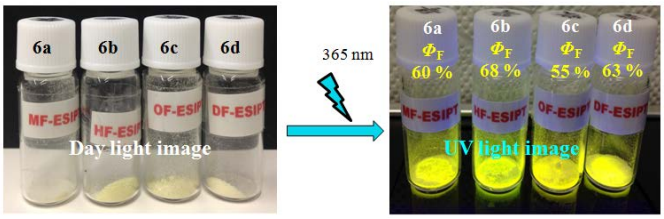


**Fig. 4** Day light and UV light images of compounds **6a-6d**.

A third emission band at 430 nm was also observed along with normal ESIPT process emissions in acetonitrile due to protonated *cis–enol*. Similar spectral observations were observed for all compounds in methanol solvent.

Compounds are highly emissive in solid state and weakly emissive in solvents of different polarity after photoexcitation. This quenching in fluorescence in solution can be assigned to intramolecular rotation or conformational changes due to solvation effect[80]. The compounds **6a-6d** are yellow colored emissive in solid state upon photoexcitation (**Fig. 4**). The compound **6a** showed broad emission maxima at 544 nm, which is blue shifted emission as compared to **6b** ($\lambda_{em}$ = 551 nm), **6c** ($\lambda_{em}$ = 552 nm) and **6d** ($\lambda_{em}$ = 552 nm).

Recently Wang and coworkers reported ultra–high quantum yield (91.68%) in solid state with desirable Stokes shift for carbazole based hydroxy benzothiazole ESIPT derivative[69]. A large Stokes shift is a desirable property of the compounds having ESIPT unit[42]. Remarkably large Stokes shift was observed for the compounds **6a–6d** in solid state as well as in solution. In solid state, Stokes shift was higher for **6c** (11,645 $cm^{-1}$) in comparison to **6d** (11,382 $cm^{-1}$), **6b** (11,436 $cm^{-1}$) and **6a** (10,687 $cm^{-1}$). Similar Stokes shifts were observed in solvents of different polarity (**Table 1**). Interestingly, here along with large Stokes shift we have achieved very high quantum efficiencies by incorporating rigid fluorene core between two benzothiazole units. Compound **6b** showed highest absolute quantum yield (67.21%) as compared to **6d** (62.94%), **6a** (60.12%) and **6c** (54.65%) in solid state. The high quantum yields in solid state can be assigned to slip–stacking and strong intramolecular hydrogen bonding[22]. The 10–15 fold quenching in quantum efficiency was observed in solution as compared to solid state. The relative quantum yields of compounds were studied in chloroform, toluene and DMF at different concentrations. Except in DMF (for **6a** and **6b**), at lower concentration compounds showed high quantum efficiency. In DMF, the quantum yields were almost same for $10^{-5}$ and $10^{-6}$ M concentration for all compounds except **6c**. Compound **6c** showed 1.5 fold more quantum yield at $10^{-6}$ M concentration in comparison to $10^{-5}$ M concentration. However, **6a** and **6b** showed more quantum yields at $10^{-5}$ M concentration in comparison to $10^{-6}$ M concentration. In chloroform and toluene, 3–4 fold enhancement in quantum yields were observed for dilute solution. In short, compounds showed higher quantum yields in DMF in comparison to chloroform and toluene. Lowering of quantum yields in chloroform can be assigned to quenching effect of heavy chlorine atoms and ACQ in toluene by observing fluorescence color.

A detailed study was carried out to study the effect of phase transition or polymorphism (upon heating) on fluorescence properties. In further experiment, spin coated samples **6a-6d** were heated up to 250 °C slowly, and the emission spectra were recorded in molten state as it cooled to room temperature (20 °C). The emission spectra were similar in molten state and crystalline state. In both the states the compounds emit at same wavelength with change in the fluorescence intensity (**Fig.** 5).

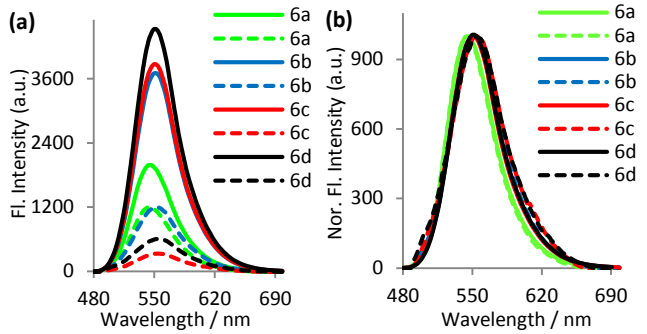


**Fig. 5** Steady state emission spectra of compounds **6a-6d** in crystalline state and molten state (a) Fluorescence spectra in solid state (solid line) and molten state (dotted line) (b) Normalized fluorescence spectra in solid state (solid line) and molten state (dotted line), (concentration 1 wt %, λex = 330 nm).

**Time–resolved fluorescence measurements**

The fluorescence lifetimes in chloroform solution and in solid state were evaluated by monitoring the peak at 552 nm upon 377 nm excitation (**Fig. 6** and **Fig. S3**). The fluorescence decays were fitted to a multi (bi or tri)–exponential decay function. The average lifetimes of **6a** ($\Phi_F$ = 1.8%), **6b** ($\Phi_F$ = 1.8%), **6c** ($\Phi_F$ = 1.7%) and **6d** ($\Phi_F$ = 1.6%) in chloroform were 0.52, 0.74, 0.75 and 0.55 ns respectively (**Table 2**). In contrast, all of the ESIPT molecules showed 5–10 times longer lifetime in solid state than those in the solutions, **6a** ($\Phi_F$ = 60.12; $\tau_F$ = 5.21 ns), **6b** ($\Phi_F$ = 67.21; $\tau_F$ = 3.56 ns), **6c** ($\Phi_F$ = 54.65; $\tau_F$ = 3.48 ns), and **6d** ($\Phi_F$ = 62.94; $\tau_F$ = 3.15 ns). Interestingly, the decays in solutions were mostly dominated by the single exponential function (78–89%), while those in the solid states were partly composed of primary bi–exponential functions (48–78%). In particular, **6b** and **6d** indicate almost equal contributions of ca. 4.5–4.8 ns and 2.7–3.1 ns decays. Based on the steady–state electronic absorption properties summarized in **Table 1**, radiative lifetimes $\tau_R$ from the compounds are calculated as $\tau_R$ = 0.54, 0.53, 0.58, 0.51 for **6a, 6b, 6c**, and **6d**, respectively based on their oscillator strength *f* estimated by the numerical integrations of their steady state absorption spectra. The relative strength of *f* (= 2.9, 3.0, 2.7, and 3.1 respectively) for **6a, 6b, 6c**, and **6e** in these series of compounds was well represented by the TD–DFT calculations (*f* = 1.1, 0.8, and 1.2, respectively for **6b, 6c**, and **6d**) relative to **6a**. The values of $\tau_R$ are consistent with fluorescence lifetimes in solutions (**Table 1**). In the solid state, the lifetime exhibit considerable elongation up to 5 ns, suggesting that the emission can be attributed to the keto forms with the smaller polarizability (ESIPT emission) through relatively slow structural relaxation from the ground state enol form.

**Aggregation Induced Emission (AIE) study**

In order to have more information about fluorescence properties in the aggregate state, AIE study was performed for representative compound **6b** in THF and THF–water mixture (various ratios).

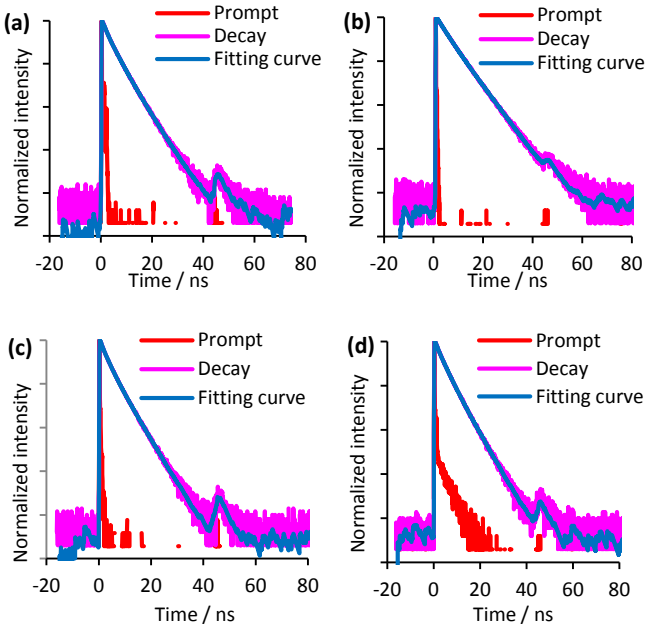


**Fig. 6** Time resolved fluorescence decays of compounds in solid state (a) **6a** (b) **6b** (c) **6c** (d) **6d** (λex : 377 nm).

**Table 2:** Summary of excited state lifetimes (a) solid state (b) in chloroform of compounds **6a–6d**

| Comps. | $\tau_1$/ns ($A_1$ %) | $\tau_2$/ns ($A_2$%) | $\tau_3$/ns ($A_3$ %) | Average $\tau_F$ (ns) |
|---|---|---|---|---|
| [a]6a | 5.75 (78) | 3.31 (22) | - | 5.21 |
| [b]6a | 0.57 (88) | 0.13 (12) | - | 0.52 |
| [a]6b | 3.06 (48) | 4.82 (42) | 0.68 (10) | 3.56 |
| [b]6b | 0.60 (78) | 0.23 (13) | 2.89 (9) | 0.74 |
| [a]6c | 4.22 (65) | 2.14 (32) | 0.34 (3) | 3.48 |
| [b]6c | 0.52 (89) | 2.56 (11) | - | 0.75 |
| [a]6d | 4.56 (48) | 2.70 (47) | 0.63 (5) | 3.15 |
| [b]6d | 0.60 (84) | 0.25 (16) | - | 0.55 |

The absorption and emission spectra of **6b** in THF and THF–water mixture at different water fractions are shown in **Fig. 7**. In THF solution, **6b** showed dual emissions at 404 and 553 nm corresponding to the enol (E*) and keto (K*) emission respectively. Upon increasing water fraction from 0 to 60 %, a slight change was observed in fluorescence intensity. This slight shift is not due to aggregation but caused by the solvent effect[31,81,82]. When the water fraction was further increased from 70 to 90%, the significant change in the absorption and emission spectra were observed. The sudden change in the emission and absorption spectra becomes the evidence for the formation of nano-particles[31,81,82]. This sudden spectral change indicates the transition from the homogenous solution to the nanoaggregates and is not due to solvent effect[81,82]. When the water fraction is between 0–60 %, the absorption peaks are almost identical at around 334 nm, similar to absorption peak in THF solution.

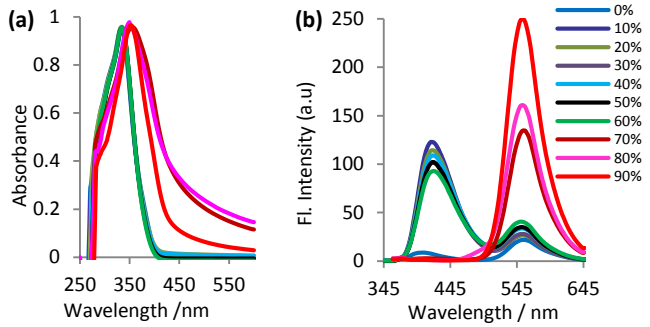


**Fig. 7** (a) Normalized absorption spectra (b) Steady state emission spectra of compound **6b** in THF and THF-water mixture (Concentration $10^{-5}$ M concentration, room temperature, λex = 330 nm, water fraction (vol %)).

However, in fluorescence spectra the intensity of enol and keto emission is comparatively higher as compared to emission peaks in THF. In aggregated state (water 70–90 %), 20 nm red shift in absorption was observed. This red shift is assigned to *J*–aggregation which is a typical characteristic of AIE[20]. The formation of *J*–aggregates was further conformed by single crystal data. In the aggregate state, the enol emission around 415–420 nm gradually disappeared and keto emission (554 nm) became the dominant emission. The maximum fluorescence efficiency was obtained at 90 % water content, upto 7 fold enhancements ($\Phi_F$ = ~ 10) in quantum efficiency was observed in aggregate state in comparison to molecularly dispersed THF solution ($\Phi_F$ = 1.5).

**Structural Properties**

To have further in depth knowledge of structural properties of compounds, differential scanning calorimetry (DSC), thermogravimetric analysis (TGA), powder–XRD and single X–ray analyses were carried out. DSC analyses were performed on the neat material under nitrogen atmosphere. The summarized results of DSC are shown in **Fig. S4**.

On the first heating cycle by differential scanning colorimeter, very sharp melting endothermic transitions were observed for **6b**, **6c** and **6d**. The compound **6a** did not show endothermic transition up to 300 °C for both cycles of DSC. The melting transitions were observed at 216 °C, 175 °C and 135 °C for **6b**, **6c** and **6d** respectively, which indicates presence of molecular order within the crystalline state. In case of **6d** small endothermic peaks were observed (at 36 °C and 76 °C) before melting endothermic transition. These can be assigned to slight disorder (or phase change) in the crystalline state. After melting, crystalline materials undergo phase transition to isotropic liquid. The materials then appear to become kinetically trapped in the amorphous phase (glass state). Phase transition was not observed upon cooling to room temperature (no recrystallisation occurs) in first DSC cycle for **6c** and **6d**. Compound **6b** showed small phase transition peak at 30 °C in first cooling cycle. This is due to slight change in amorphous phase. In second cycle of DSC, melting endothermic transition was not observed for **6c** and **6d** upon heating. This clearly indicates that materials remain in glass state after first melting endothermic transition. In case of **6b**, board exothermic phase transition (160 °C) was observed before melting endothermic transition (216 °C). This transition is a phase change from glass state to crystalline state (recrystallisation occur in second DSC heating cycle). After melting endothermic transition, **6b** remained in glass state after cooling. Similar to first cooling cycle, small phase transition peak was observed at 37 °C for second cooling cycle for **6b**. The DSC data concludes that phase transition of the materials is irreversible in nature for **6c** and **6d**, but it is reversible for **6b**. The compounds **6a**–**6d** are crystalline in nature which were confirmed by powder–XRD experiments **Fig. S5**.

Thermogravimetric analysis (TGA) technique is used for evaluation of thermal stability of emissive compounds. Thermogravimetric analysis were carried out under nitrogen atmosphere using alumina/ Pt pans at the ramp rate of 10 °C/min for temperature range between 40 to 1000 °C. Compounds **6a-6d** are thermally stable up to 400 °C. The compounds **6b** and **6d** showed 5% weight loss at 415 °C while, **6a** and **6c** showed 5% weight loss at 424 °C. The degradation of compounds started after 415 °C, and significant weight loss was observed between 415–540 °C, however after 540 °C the % weight loss was very slow. Except **6c**, 80% degradation was observed around 540 °C for the compounds. Compound **6c** showed 70% degradation up to 550 °C and did not degrade completely even up to 1000 °C (75% weight loss observed) and other compounds showed 87–95% weight loss at 1000 °C. The TGA data clearly indicates that the $T_d$ is not dependent on length of alkyl chain attached to 9,9–position of fluorene. The high thermal stability is due to the rigid fluorene and benzothiazole unit. Overall, all compounds showed almost same and very high thermal stability. The thermal stability data are summarized in **Fig. S6**.

X–Ray crystallographic analysis of **6b** was performed (other compounds we are unable to obtained single crystal ever after many attempts) to study structural parameters. The crystal structure of **6b** is shown in **Fig. 8**, **Fig. S7** and **Table S1.**

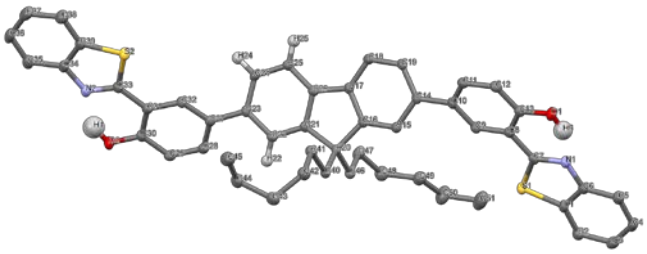

**Fig. 8** X–ray crystal structure of **6b**. Hydrogen atoms (except for –OH groups) are omitted for clarity. Thermal ellipsoids are set at 50% probability. Hydrogen atoms except OH groups were restrained to ride on the atom to which they are bonded. The two OH hydrogen atoms were put by using reflection data.

The distances between the oxygen and nitrogen ($O_1$–$N_1$ and $O_2$–$N_2$) were 2.593 Å and 2.612 Å respectively, indicating the formation of an intramolecular hydrogen bond ($O_1$–$H_6$---$N_1$ and $O_2$–$H_1$---$N_2$). The O–H bond lengths of phenolic hydoxy group ($O_1$–$H_6$ and $O_2$–$H_1$) were 0.881 Å and 0.910 Å respectively. The bond lengths between acidic hydrogen atoms and basic nitrogen atoms (intramolecular hydrogen bonds; $N_1$–$H_6$ and $N_2$–$H_1$) were 1.788 Å for each bond. The small torsion angle between the two aromatic rings was ($N_1$–$C_7$–$C_8$–$C_{13}$ and $N_2$–$C_{33}$–$C_{31}$–$C_{30}$) 4.5° and 2.5° respectively, confirming the coplanar configuration which fulfills the requirement of ESIPT (**Fig. S7**). A small twisting ($C_{11}$–$C_{10}$–$C_{14}$–$C_{19}$ and $C_{32}$–$C_{27}$–$C_{23}$–$C_{24}$, 39° and 36° respectively) was observed between fluorene and hydroxy benzothiazole (HBT) in the crystal. The crystal had slip–stacked packing with interplanar distance of about 3.617 Å (**Fig. S7**). The 2–(2–hydroxyphenyl) benzothiazole part of molecule overlapped with phenyl and imidazole part of the neighboring molecule. The distance between an oxygen atom and the nearest nitrogen atom ($O_1$–$N_1$) of neighboring molecule was 4.756 Å, which confirms the absence of inter–molecular hydrogen bonding (**Fig. S7**). The high quantum yields can be explained by conformational fixating in the photo–excited state due to strong intramolecular hydrogen bonding which suppresses the molecular rotation and non–radiative decay[22].

**Theoretical calculation**

**Geometric structure**

The compounds **6a**–**6d** contains two HBT units separated by fluorene motif. In order to study the proton transfer process in detail, DFT computations were performed[83]. The ground and excited state of *cis–enol* were optimized using B3LYP functional and 6-31G**(d,p) basis set. Theoretical calculation was carried out for the *cis–enol* form for **6a** (small alkyl chain compound was considered for simplicity). In the ground state, the O–H bond length of phenolic hydoxy group ($O_{27}$–$H_{57}$ and $O_{41}$–$H_{65}$) was found to be 0.992 Å. At the same time, the bond lengths between acidic hydrogen atoms and basic nitrogen atoms (intramolecular hydrogen bond; $N_{74}$–$H_{57}$ and $N_{75}$–$H_{65}$) were found to be 1.733 Å. At the excited state ($S_1$ state), the O–H bond lengths ($O_{27}$–$H_{57}$ and $O_{41}$–$H_{65}$) extended to 1.022 Å and 0.998 Å respectively, while N–H ($N_{74}$–$H_{57}$ and $N_{75}$–$H_{65}$) bond lengths decreased to 1.611 Å and 1.706 Å respectively (**Fig. S8**). The increase in O–H bond lengths and the decrease in N–H bond lengths suggest the increase in intramolecular hydrogen bond strength at $S_1$ state, which favor ESIPT process. However the shorting of (N–H) distance and elongation of bond length (O–H) in the $S_1$ state is more dramatic on one side than the other (**Table 3**).

**Table 3**. Calculated bond lengths (Å) and angles (°) of **6a** in the $S_0$ and $S_1$ states

| Bond lengths/ angle | Electronic State | | Bond lengths/ angle | Electronic State | |
|---|---|---|---|---|---|
| | $S_0$ | $S_1$ | | $S_0$ | $S_1$ |
| $O_{27}$–$H_{57}$ | 0.992 | 1.022 | $O_{41}$–$H_{65}$ | 0.992 | 0.998 |
| $N_{74}$–$H_{57}$ | 1.733 | 1.611 | $N_{75}$–$H_{65}$ | 1.733 | 1.706 |
| δ($O_{27}$–$H_{57}$–$N_{74}$) | 147.0 | 151.6 | δ($O_{41}$–$H_{65}$–$N_{75}$) | 147.0 | 147.2 |

The concomitant enlargement of the $O_{27}$–$H_{57}$–$N_{74}$ angle from 147° in the $S_0$ state to 151° in the $S_1$ state indicate that strong intramolecular hydrogen bond is strengthened in the $S_1$ state. Moreover, in the case of $O_{41}$–$H_{65}$–$N_{75}$ angle enlargement of bond angle is not significant. This result clearly indicates that proton transfer in the excited state is not occurs simultaneously for both HBT units [84–86]. This observation is supported by degenerate LUMOs energies in next section. Similar to single crystal data, the calculated torsion angles $N_{74}$–$C_{20}$–$C_{18}$–$C_{17}$ and $N_{75}$–$C_{34}$–$C_{32}$–$C_{31}$ (phenyl and imidazole ring) at ground state were 0.4 and 0.2° respectively, which support the experimental results about planarity between phenyl and benzothiazole unit. The computed dihedral angles between the fluorene and HBT unit $C_{15}$–$C_{14}$–$C_{11}$–$C_{12}$ and $C_{33}$–$C_{28}$–$C_2$–$C_1$ were 37° each at ground state, which is in accordance with experimental results. In the $S_1$ state, the computed dihedral angles $C_{15}$–$C_{14}$–$C_{11}$–$C_{12}$ and $C_{33}$–$C_{28}$–$C_2$–$C_1$ were 23° and 29° respectively, implying that compound is more planar in the excited state in comparison to ground state. The experimental and computed dihedral angle values of compounds clearly indicate that compounds have efficient conjugation between the fluorene core and HBT units.

**Frontier molecular orbitals**

Photoelectron yield spectroscopy (PYS) was used for experimental HOMOs level determination of the compounds **6a–6d** (**Fig. S9**). All the compounds showed a comparatively same HOMO level (**Fig. S10, Table 4**). The compound **6c** showed a slightly deeper **HOMO** level (-6.06 eV) in comparison to **6d** (-6.00 eV), **6b** (-6.00 eV), and **6a** (-6.02 eV). The deeper **HOMO** level of the compounds is due to two electron withdrawing benzothiazole units attached to fluorene unit. The LUMO levels of the compounds **6a–6d** were calculated from HOMO energy levels and optical band gap ($E_g^{opt}$). The optical band gaps of the compounds were calculated from the onset value of thin film UV–Vis absorption spectrum. The $E_g^{opt}$ were found to be 3.09, 3.19, 3.18 and 3.19 eV for **6a**, **6b**, **6c** and **6d** respectively. The LUMO level of compounds is similar to HOMO level (**Fig. S10**, **Table 4**). The LUMO of **6a** and **6d** were found to be -2.97 eV, and **6b** and **6c** showed decreased LUMO levels (-2.81 and -2.88 eV respectively) in comparison to **6a** and **6d**. The energy gap between HOMO and LUMO is almost same for all the compounds due to similar backbone of the compounds. Results indicate that alkyl change attached to fluorene core did not involve significantly in electron distribution.

In order to have more understanding of the nature of the electronically excited state, the calculated MOs of **6a** are shown in **Fig. 9**. Only the highest occupied molecular orbital and degenerate lowest unoccupied molecular orbitals are shown here. **Fig. 9** illustrates that the HOMO and the LUMO are localized on different part of the **6a**. In **HOMO** the electron density is concentrated on fluorene motif, while the electron density is distributed over benzothiazole for **LUMO** and degenerate **LU+1MO** orbitals.

**Table 4.** Absorption maxima, band gap and HOMO/LUMO energies of compounds **6a-6d**

| Comp | $\lambda_{max}^{Abs}$ thin film [a] (nm) | Onset [a] (nm) | $E_g^{opt}$ (eV) [b] | HOMO Expt. [c] [Calc.] [d] (eV) | LUMO Expt. [e] [Calc.] [d] (eV) |
|---|---|---|---|---|---|
| **6a** | 344 | 401 | 3.09 | -6.02 [-5.25] | -2.97 [-1.74] |
| **6b** | 338 | 389 | 3.19 | -6.00 [-5.25] | -2.81 [-1.74] |
| **6c** | 336 | 389 | 3.18 | -6.06 [-5.25] | -2.88 [-1.74] |
| **6d** | 339 | 389 | 3.19 | -6.00 [-5.25] | -2.97 [-1.74] |

[a] Prepared on quartz plate by spin–casting of dichloromethane compounds solution (1 wt %). [b] Determined by onset of optical absorption. [c] Measured by photoelectron yield spectroscopy. [d] DFT calculation by B3LYP/6-31G**(d,p) during DFT calculation side alkyl chains were replaced by methyl group for simplicity. [e] Calculated by adding $E_g^{opt}$ to HOMO.

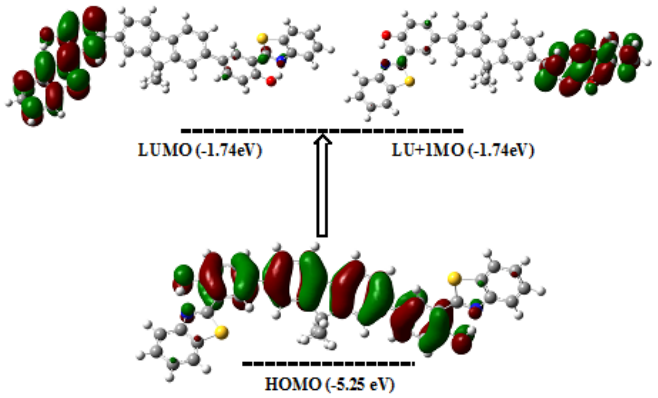


**Fig. 9** Frontier molecular orbitals (HOMO, LUMO and LU+1MO) of **6a** (*Enol* form).

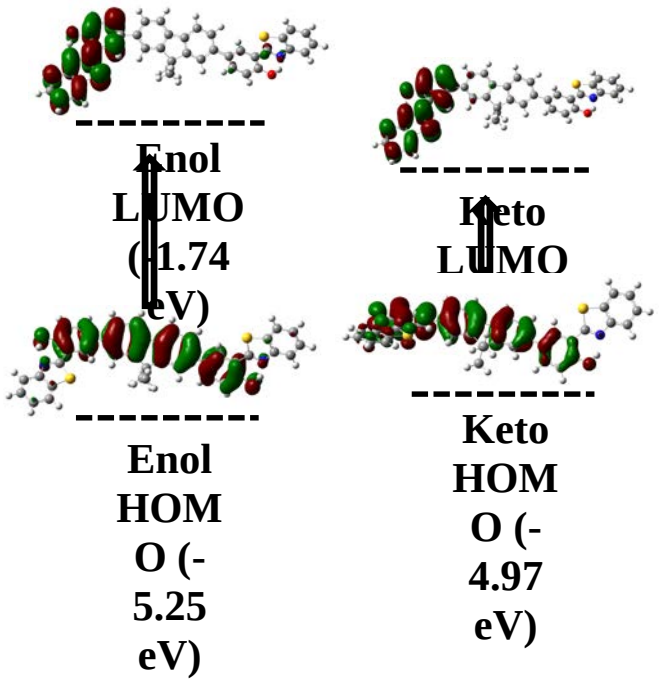


**Fig. 10** Frontier molecular orbitals with energies (HOMO and LUMO) of **6a** (Enol and Keto form).

This clearly indicates that charge transfer from fluorene core to benzothiazole unit resulted after photo–excitation on both side of HBT units. The energies of **LUMO** and **LU+1MO** conclude that change of charge density takes place with equal probability but not simultaneously. The experimental results of HOMO and LUMO energies are well in agreement with theoretical results computed by DFT.

The HOMO and LUMO energies of the **6a** were evaluated for both *enol* and *keto* form **Fig. 10**. The *enol* form showed deeper HOMO level in comparison to HOMO level of *keto* form, while LUMO of *keto* form is deeper than that of *enol* form. There is large orbital energy difference between HOMOs and LUMOs of *enol* and *keto*. This condition is not favorable for effective orbital interaction between excited state *enol* and ground state *keto* form[59,87]. The energy transfer from excited state *keto* to ground state *enol* is forbidden due to large mismatch of their molecular orbital's energy levels. This suppressed the fluorescence quenching process leading to high quantum yields.

## Conclusion

In summary, we have succeeded in preparation of solid state emissive compounds by tuning 2–(2'–hydroxy) benzothiazole unit by facial and straight forward chemical alteration. Very high quantum efficiency (~ 68%) of small fluorene based ESIPT molecules is a very striking feature of the present protocol. The X–ray single crystal analysis and DFT computations confirm the suitability of ESIPT process. Intra–molecular charge transfer nature between the donor (fluorene) and the ESIPT acceptor molecules conduct the large mismatch of HOMO and LUMO levels in their ground and excited states, leading to the design of ESIPT based highly emissive solid state compounds. High

 

quantum yield, large Stokes shift, micro–environmental sensitive emission, high fluorescence life time together with their known structural properties, make these materials exciting candidates for many solid state optoelectronic applications.

## Acknowledgments

We deeply thank Dr. Nobuko Kanehisa (Osaka University, Japan) for her help in single–crystal X–ray analysis, Professor Satoshi Minakata (Osaka University, Japan) for thermogravimetric analysis. V. S. P. and D.S. thanks the JSPS Research Fellowship. This work was partly supported by a Grant-in-Aid for Scientific Research (No. 26102011, 26810023, 2604063, 26102001) from the Japan Society for the Promotion of Science (JSPS).

## Notes and references

1 H. Nakanotani, T. Higuchi, T. Furukawa, K. Masui, K. Morimoto, M. Numata, H. Tanaka, Y. Sagara, T. Yasuda and C. Adachi, *Nat. Commun.*, 2014, **5**, 4016.
2 T. M. Figueira-Duarte and K. Müllen, *Chem. Rev.*, 2011, **111**, 7260–7314.
3 A. Mishra and P. Bäuerle, *Angew. Chemie - Int. Ed.*, 2012, **51**, 2020–2067.
4 Y. S. Zhao, H. Fu, A. Peng, Y. Ma, Q. Liao and J. Yao, *Acc. Chem. Res.*, 2010, **43**, 409–418.
5 F. Gao, Q. Liao, Z. Z. Xu, Y. H. Yue, Q. Wang, H. L. Zhang and H. B. Fu, *Angew. Chemie - Int. Ed.*, 2010, **49**, 732–735.
6 I. D. W. Samuel and G. A. Turnbull, *Chem. Rev.*, 2007, **107**, 1272–1295.
7 M. Irie, T. Fukaminato, T. Sasaki, N. Tamai and T. Kawai, *Nature*, 2002, **420**, 759–760.
8 M. E. Cinar and T. Ozturk, *Chem. Rev.*, 2015, **115**, 3036–3140.
9 X. Ban, W. Jiang, K. Sun, X. Xie, L. Peng, H. Dong, Y. Sun, B. Huang, L. Duan and Y. Qiu, *ACS Appl. Mater. Interfaces*, 2015, **7**, 7303–7314.
10 X. Du, J. Qi, Z. Zhang and Z. Y. Wang, *Chem. Mater.*, 2012, **24**, 2178–2185.
11 H. Sasabe and J. Kido, *Chem. Mater.*, 2011, **23**, 621–630.
12 T. Ozdemir, S. Atilgan, I. Kutuk, L. T. Yildirim, A. Tulek, M. Bayindir and E. U. Akkaya, *Org. Lett.*, 2009, **11**, 2105–2107.
13 W. Sun, S. Li, R. Hu, Y. Qian, S. Wang and G. Yang, *J. Phys. Chem. A*, 2009, **113**, 5888–5895.
14 Y. Li, G. Zhang, G. Yang, Y. Guo, C. Di, X. Chen, Z. Liu, H. Liu, Z. Xu, W. Xu, H. Fu and D. Zhang, *J. Org. Chem.*, 2013, **78**, 2926–2934.
15 L. Li, S. Zhang, L. Han, Z. Sun, J. Luo and M. Hong, *Cryst. Growth Des.*, 2013, **13**, 106–110.
16 J. Brunel, O. Mongin, A. Jutand, I. Ledoux, J. Zyss and M. Blanchard-Desce, *Chem. Mater.*, 2003, **15**, 4139–4148.
17 M. Goel, K. Narasimha and M. Jayakannan, *J. Phys. Chem. B*, 2015, **119**, 5102–5112.
18 X. Zhang, X. Zhang, S. Wang, M. Liu, Y. Zhang, L. Tao and Y. Wei, *ACS Appl. Mater. Interfaces*, 2013, **5**, 1943–1947.
19 N. Yanai, K. Kitayama, Y. Hijikata, H. Sato, R. Matsuda, Y. Kubota, M. Takata, M. Mizuno, T. Uemura and S. Kitagawa, *Nat. Mater.*, 2011, **10**, 787–793.
20 Y. Hong, J. W. Y. Lam and B. Z. Tang, *Chem. Soc. Rev.*, 2011, **40**, 5361–5388.
21 T. Mutai, H. Sawatani, T. Shida, H. Shono and K. Araki, *J. Org. Chem.*, 2013, **78**, 2482–2489.
22 J. E. Kwon and S. Y. Park, *Adv. Mater.*, 2011, **23**, 3615–3642.
23 R. Rao M, C.-W. Liao, W.-L. Su and S.-S. Sun, *J. Mater. Chem. C*, 2013, **1**, 5491–5501.
24 A. Maity, F. Ali, H. Agarwalla, B. Anothumakkool and A. Das, *Chem. Commun.*, 2015, **51**, 2130–2133.
25 J. Li, Y. Qian, L. Xie, Y. Yi, W. Li and W. Huang, *J. Phys. Chem. C*, 2015, **119**, 2133–2141.
26 X. Wang, J. Hu, G. Zhang and S. Liu, *J. Am. Chem. Soc.*, 2014, **136**, 9890–9893.
27 C. W. T. Leung, Y. Hong, S. Chen, E. Zhao, J. W. Y. Lam and B. Z. Tang, *J. Am. Chem. Soc.*, 2013, **135**, 62–65.
28 C. Y. K. Chan, Z. Zhao, J. W. Y. Lam, J. Liu, S. Chen, P. Lu, F. Mahtab, X. Chen, H. H. Y. Sung, H. S. Kwok, Y. Ma, I. D. Williams, K. S. Wong and B. Z. Tang, *Adv. Funct. Mater.*, 2012, **22**, 378–389.
29 Y. Shigemitsu, T. Mutai, H. Houjou and K. Araki, *J. Phys. Chem. A*, 2012, **116**, 12041–12048.
30 T. Mutai, H. Satou and K. Araki, *Nat. Mater.*, 2005, **4**, 685–687.
31 M. Cai, Z. Gao, X. Zhou, X. Wang, S. Chen, Y. Zhao, Y. Qian, N. Shi, B. Mi, L. Xie and W. Huang, *Phys. Chem. Chem. Phys.*, 2012, **14**, 5289–5296.
32 T. H. Kim, M. S. Choi, B.-H. Sohn, S.-Y. Park, W. S. Lyoo and T. S. Lee, *Chem. Commun. (Camb).*, 2008, **1**, 2364–2366.
33 J. Luo, Z. Xie, J. W. Lam, L. Cheng, H. Chen, C. Qiu, H. S. Kwok, X. Zhan, Y. Liu, D. Zhu and B. Z. Tang, *Chem. Commun. (Camb).*, 2001, **381**, 1740–1741.
34 T. Mutai, H. Tomoda, T. Ohkawa, Y. Yabe and K. Araki, *Angew. Chemie - Int. Ed.*, 2008, **47**, 9522–9524.
35 M. K. Nayak, B. H. Kim, J. E. Kwon, S. Park, J. Seo, J. W. Chung and S. Y. Park, *Chem. - A Eur. J.*, 2010, **16**, 7437–7447.
36 Y. Qian, M. M. Cai, L. H. Xie, G. Q. Yang, S. K. Wu and W. Huang, *ChemPhysChem*, 2011, **12**, 397–404.
37 A. H. Shelton, I. V. Sazanovich, J. A. Weinstein and M. D. Ward, *Chem. Commun.*, 2012, **48**, 2749.
38 E. Wang, J. W. Y. Lam, R. Hu, C. Zhang, Y. S. Zhao and B. Z. Tang, *J. Mater. Chem. C*, 2014, **2**, 1801–1807.
39 D.-E. Wu, Q.-C. Yao and M. Xia, *Phys. Chem. Chem. Phys.*, 2015, **17**, 3287–3294.
40 B. Xu, J. Zhang, H. Fang, S. Ma, Q. Chen, H. Sun, C. Im and W. Tian, *Polym. Chem.*, 2014, **5**, 479–488.
41 M. Yang, D. Xu, W. Xi, L. Wang, J. Zheng, J. Huang, J. Zhang, H. Zhou, J. Wu and Y. Tian, *J. Org. Chem.,* 2013, **78**, 10344–10359.
42 J. Zhao, S. Ji, Y. Chen, H. Guo and P. Yang, *Phys. Chem. Chem. Phys.*, 2012, **14**, 8803–8817.
43 J. Wu, W. Liu, J. Ge, H. Zhang and P. Wang, *Chem. Soc. Rev.*, 2011, **40**, 3483–3495.
44 C.-C. Hsieh, C.-M. Jiang and P.-T. Chou, *Acc. Chem. Res.*, 2010, **43**, 1364–1374.
45 O. K. Abou-Zied, R. Jimenez, E. H. Z. Thompson, D. P. Millar and F. E. Romesberg, *J. Phys. Chem. A*, 2002, **106**, 3665–3672.
46 P. Majumdar and J. Zhao, J. *Phys. Chem. B* 2014, **119**, 2384–2394.
47 T. Iijima, A. Momotake, Y. Shinohara, T. Sato, Y. Nishimura and T. Arai, *J Phys. Chem. A*, 2010, **05**, 1603–1609.
48 J. Cheng, D. Liu, L. Bao, K. Xu, Y. Yang and K. Han, *Chem. - An Asian J.*, 2014, **9**, 3215–3220.
49 K.-C. Tang, M.-J. Chang, T.-Y. Lin, H.-A. Pan, T.-C. Fang, K.-Y. Chen, W.-Y. Hung, Y.-H. Hsu and P.-T. Chou, *J. Am. Chem. Soc.*, 2011, **133**, 17738–17745.

50 H. Shono, T. Ohkawa, H. Tomoda, T. Mutai and K. Araki, *ACS Appl. Mater. Interfaces*, 2011, **3**, 654–657.
51 B. Liu, H. Wang, T. Wang, Y. Bao, F. Du, J. Tian, Q. Li and R. Bai, *Chem. Commun.*, 2012, **48**, 2867–2869.
52 O. M. Zamotaiev, V. Y. Postupalenko, V. V. Shvadchak, V. G. Pivovarenko, A. S. Klymchenko and Y. Mély, *Bioconjug. Chem.*, 2011, **22**, 101–107.
53 G.-J. Zhao and K.-L. Han, *Acc. Chem. Res.*, 2012, **45**, 404–413.
54 T.-H. Kim, H. K. Lee, O. O. Park, B. D. Chin, S.-H. Lee and J. K. Kim, *Adv. Funct. Mater.*, 2006, **16**, 611–617.
55 V. Luxami and S. Kumar, *New J. Chem.*, 2008, **32**, 2074–2079.
56 J. Lee, C. H. Kim and T. Joo, *J. Phys. Chem. A*, 2013, **117**, 1400–1405.
57 W.-T. Chuang, C.-C. Hsieh, C.-H. Lai, C.-H. Lai, C.-W. Shih, K.-Y. Chen, W.-Y. Hung, Y.-H. Hsu and P.-T. Chou, *J. Org. Chem.*, 2011, **76**, 8189–8202.
58 M. Flegel, M. Lukeman, L. Huck and P. Wan, *J. Am. Chem. Soc.*, 2004, **126**, 7890–7897.
59 K. Sakai, T. Ishikawa and T. Akutagawa, *J. Mater. Chem. C*, 2013, **1**, 7866–7871.
60 T. Mutai, H. Shono, Y. Shigemitsu and K. Araki, *CrystEngComm*, 2014, **16**, 3890–3895.
61 H. Konoshima, S. Nagao, I. Kiyota, K. Amimoto, N. Yamamoto, M. Sekine, M. Nakata, K. Furukawa and H. Sekiya, *Phys. Chem. Chem. Phys.*, 2012, 16448–16457.
62 K. Furukawa, N. Yamamoto, T. Nakabayashi, N. Ohta, K. Amimoto and H. Sekiya, *Chem. Phys. Lett.*, 2012, **539-540**, 45–49.
63 H. H. G. Tsai, H. L. S. Sun and C. J. Tan, *J. Phys. Chem. A*, 2010, **114**, 4065–4079.
64 W. Chen, E. B. Twum, L. Li, B. D. Wright, P. L. Rinaldi and Y. Pang, *J. Org. Chem.*, 2012, **77**, 285–90.
65 K. Benelhadj, W. Muzuzu, J. Massue, P. Retailleau, A. Charaf-Eddin, A. D. Laurent, D. Jacquemin, G. Ulrich and R. Ziessel, *Chem. - A Eur. J.*, 2014, **20**, 12843–12857.
66 A. Ohshima, A. Momotake, R. Nagahata and T. Arai, *J. Phys. Chem. A*, 2005, **109**, 9731–9736.
67 J. Cheng, D. Liu, W. Li, L. Bao and K. Han, *J. Phys. Chem. C*, 2015, **119**, 4242–4251.
68 J. Ma, J. Zhao, P. Yang, D. Huang, C. Zhang and Q. Li, *Chem. Commun.*, 2012, **48**, 9720–9722.
69 D. Yao, S. Zhao, J. Guo, Z. Zhang, H. Zhang, Y. Liu and Y. Wang, *J. Mater. Chem.*, 2011, **21**, 3568–3570.
70 S. Liu, C. Zhong, S. Dong, J. Zhang, X. Huang, C. Zhou, J. Lu, L. Ying, L. Wang, F. Huang and Y. Cao, *Org. Electron. physics, Mater. Appl.*, 2014, **15**, 850–857.
71 Y. Huo, X. Fang, B. Huang, K. Zhang, X. Nie and H. Zeng, *Chinese J. Org. Chem.*, 2012, **32**, 1169–1185.
72 Y. Koizumi, M. Ide, A. Saeki, C. Vijayakumar, B. Balan, M. Kawamoto and S. Seki, *Polym. Chem.*, 2013, **4**, 484–494.
73 L. Ying, C.-L. Ho, H. Wu, Y. Cao and W.-Y. Wong, *Adv. Mater.*, 2014, **26**, 2459–2473.
74 M. K. Bera, C. Chakraborty, P. K. Singh, C. Sahu, K. Sen, S. Maji, A. K. Das and S. Malik, *J. Mater. Chem. B*, 2014, **2**, 4733–4739.
75 Y. H. Kim, S.-G. Roh, S.-D. Jung, M.-A. Chung, H. K. Kim and D. W. Cho, *Photochem. Photobiol. Sci.*, 2010, **9**, 722–729.
76 P.-T. Chou, W. C. Cooper, J. H. Clements, S. L. Studer and C. Pin Chang, *Chem. Phys. Lett.*, 1993, **216**, 300–304.
77 J. Durmis, M. Karvas and M. Manasek, *Collect. Czech. Chem. Commun.*, 1973, **38**, 215–224.
78 M. Taneda, Y. Kodama, Y. Eda, H. Koyama and T. Kawato, *Chem. Lett.*, 2007, **36**, 1410–1411.
79 W. Frey, F. Laermer and T. Elsaesser, *J. Phys. Chem.*, 1991, **1**, 10391–10395.
80 F. A. S. Chipem, A. Mishra and G. Krishnamoorthy, *Phys. Chem. Chem. Phys.*, 2012, **14**, 8775–8790.
81 J. Chen, C. C. W. Law, J. W. Y. Lam, Y. Dong, S. M. F. Lo, I. D. Williams, D. Zhu and B. Z. Tang, *Chem. Mater.*, 2003, **15**, 1535–1546.
82 A. Patra, N. Hebalkar, B. Sreedhar, M. Sarkar, A. Samanta and T. P. Radhakrishnan, *Small*, 2006, **2**, 650–659.
83 M. Frish, H. B. Trucks, H. B. Schlegel, G. S. Scuseria, M. A. Robb, J. R. Cheeseman, G. Scalmani, V. Barone, B. Mennucci and G. A. Paterson, Guassian 09, revision 02, Inc. Wallingford CT, 2009, p34.
84 C. Qinghui, D. A. Medvetz and P. Yi, *Chem. Mater.*, 2007, **19**, 6421–6429.
85 J. Zhao, J. Chen, J. Liu and M. R. Hoffmann, *Phys. Chem. Chem. Phys.*, 2015, **17**, 11990–11999.
86 J. Zhao, H. Yao, J. Liu and M. R. Hoffmann, *J. Phys. Chem. A*, 2015, **119**, 681–688.
87 K. I. Sakai, M. Ichikawa and Y. Taniguchi, *Chem. Phys. Lett.*, 2006, **420**, 405–409.
88 S. M. Chang, K. L. Hsueh, B. K. Huang, J. H. Wu, C. C. Liao and K. C. Lin, *Surf. Coatings Technol.*, 2006, **200**, 3278–3282.


 